Wing Profile Analysis Using Lattice Gas Cellular Automata

Emanuel Schmidt, F100044

August 2, 2011

1 Introduction

As it is known since more than 150 years, the dynamics of fluids (i.e., liquids and gases) are described by the Navier-Stokes equations. A fluid is called incompressible, if $\frac{\mathrm{d}}{\mathrm{dt}}\varrho(\vec{x},t) = 0$. Given the dynamic viscosity constant μ, the equations then read

$$\varrho \cdot \left(\frac{\partial \vec{v}}{\partial t} + (\nabla \cdot \vec{v})\vec{v} \right) = -\nabla p + \mu \Delta \vec{v} + \vec{f} \tag{1}$$

$$\nabla \cdot \vec{v} = 0,$$

connecting velocity $\vec{v}(\vec{x},t)$, pressure $p(\vec{x},t)$, density $\varrho(\vec{x},t)$ and the external force density $\vec{f}(\vec{x},t)$. Solutions to these (nonlinear) equations are known only for a couple of very simple cases, and the question whether smooth, global solutions exist for smooth initial conditions is a famous open problem.

Unfortunately, using standard numerical methods is also problematic, as computing accurate solutions requires far too much computational effort and smooth behaviour of these solutions cannot be guaranteed for times larger than a characteristic blow-up time. Another approach that circumvents this problems is to model the fluid flow microscopically on a lattice, using cellular automata. In 1986, Frisch, Hasslacher and Pomeau [1] succeeded to show that a certain class of these lattice fluids (called FHP models after their inventors) indeed returns eq.(1) in the hydrodynamic limit.

In the following, a simple realization of the FHP model is used to simulate a wind tunnel and to compare the dynamic properties of three different wing profiles shown in Figure 1. The implementation was done in C under Scientific Linux, OriginPro and MATLAB were used for evaluating and plotting the data.

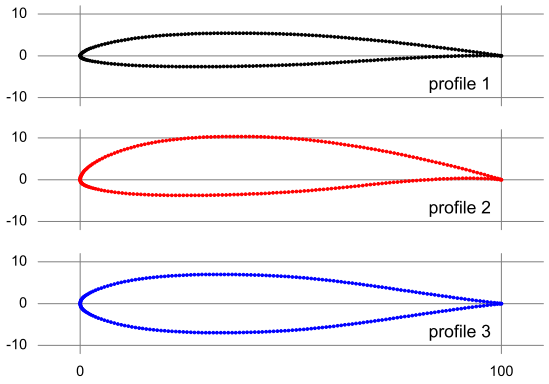

Figure 1: The three different profiles under comparison, each consisting of 200 coordinates (designed by Helmut Quadbeck for model gliders, *www.hq-modellflug.de/koordinatenframe.htm*).

2 General setup

The wind tunnel is represented by a hexagonal grid which is 800 points wide and 200 double layers high, as shown in Figure 2. In horizontal direction, periodic boundary conditions are imposed. Top and bottom are formed by reflecting surfaces, just as the 15 lamellas on the left side that stabilize the flow. The wing input data is rotated clockwise by the so-called *angle of attack* α and projected in an area of width 200. The wing points simply bounce back incoming particles instead of reflecting them, since this technique gives unique states also for curved surfaces and prevents two particles being on the same site and moving parallelly.

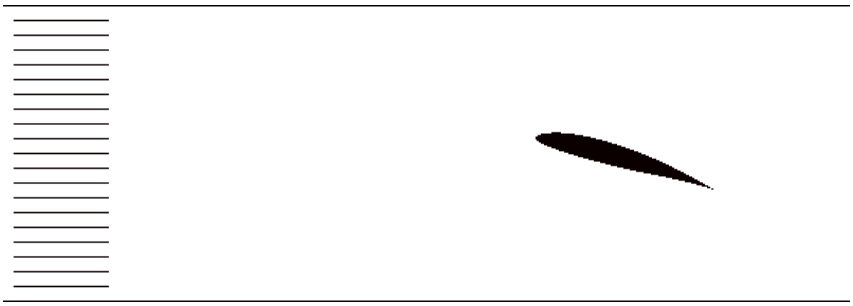

Figure 2: The wind tunnel

The grid is initialized with one particle per site (having arbitrary velocity direction), such that the macroscopic density is $\varrho = \frac{1}{6}$. In the small area to the left of the lamellas, leftward moving particles are converted into rightward moving ones with a certain probability to create a horizontal flow. The horizontal velocity is defined by adding up all horizontal velocity components and then dividing by the number of particles (not sites). The maximal reachable value for an empty tunnel containing no wing is close to 0.56, but, incorporating the wing, this value decreases and is dependent on α, as the wing represents an additional fluid resistance.

One has to make sure that the flow is stable before starting a measurement. It turns out that the horizontal velocity stabilizes after 10^5 steps in this setup, and so do the other measurands. All measurements taken in the following are then averaged over a period of another 10^5 steps.

3 Lift and drag forces

The forces acting on the wing can be evaluated easily by discretizing the fundamental relation

$$\frac{\mathrm{d}}{\mathrm{dt}}\vec{p} = \vec{F} \qquad \rightarrow \qquad \frac{\Delta\vec{p}}{\Delta t} = \vec{F}.$$

The total momentum transfer $\Delta\vec{p}$ is obtained by adding up all collisions of particles with the wing during the time interval Δt, which is simply taken to be the number of steps, $\Delta t = 10^5$. Here, one has to be aware of the fact that *twice* the momentum is transferred, and an additional factor of $\frac{\sqrt{3}}{2}$ comes into play in the vertical direction due to the grid geometry.

Firstly, the dependence of lift and drag forces on the horizontal velocity is investigated for all profiles, while $\alpha = 20°$ is kept fixed. The results are shown in Figure 3. Obviously, profile 3 produces less lift than the other two profiles, which is due to the fact that profile 3 is totally symmetric, as can be seen also from Figure 1. Indeed, it is a design for horizontal and vertical stabilizers, whereas profile 1 and profile 2 are intended as main wings.

Furthermore, it can be seen that profile 1 causes the smallest drag force as one would expect, since it is thinner than the other two profiles (that have the same percentaged maximum thickness).

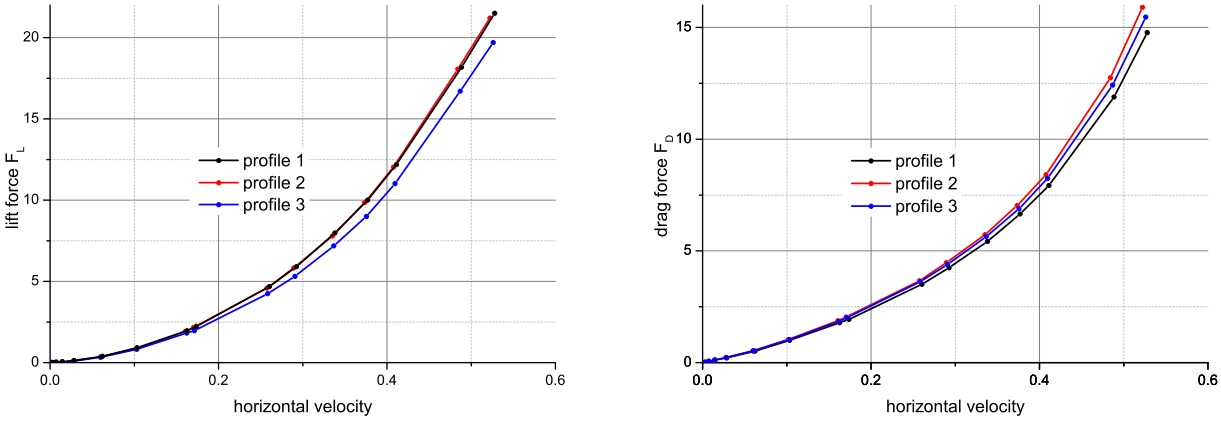

Figure 3: Lift and drag forces for different horizontal velocities, at $\alpha = 20°$.

Next, the fan strength is kept fixed, while the angle of attack α is varied. The results are shown in Figure 4. The lift forces reach a maximum and a minimum for a specific α close to $\pm 40°$, and it is notable that the curve of profile 3 is perfectly symmetric as it should be. Astonishingly, the profiles 1 and 2 produce nearly no lift at $\alpha = 0°$, which suggest that their coordinates *are given* in this way. At least, their front (leading) edges and rear (trailing) edges lie both at $y = 0$ (see Figure 1), and the overall curvature of these profiles is not very strong.

The drag forces increase with $|\alpha|$, since the area perpendicular to the wind direction gets bigger, too. This also explains why the thinner profile 1 produces less drag only at small angles, whereas the profiles 2 and 3 (having the same thickness) are behaving nearly identically except for extreme angles.

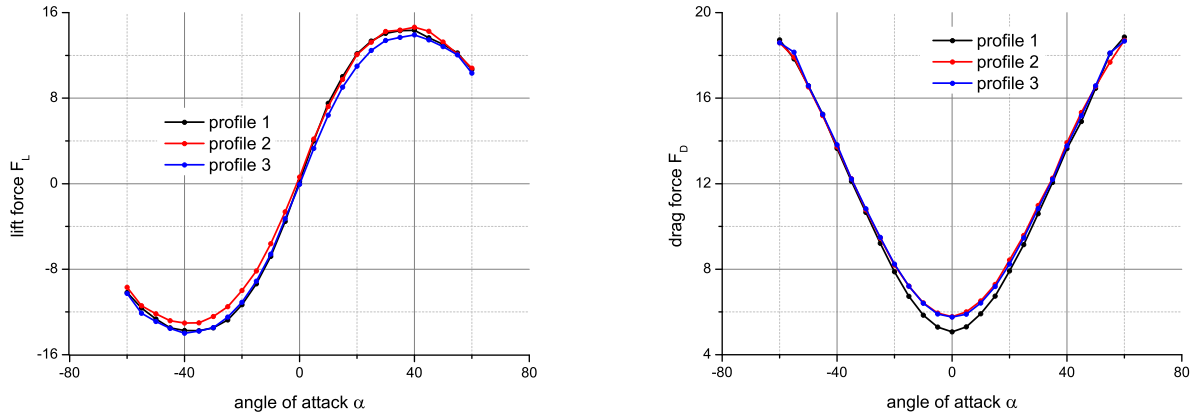

Figure 4: Lift and drag forces varying with α. The horizontal velocity is 0.45 for $\alpha = 0°$.

4 Polar diagrams

As mentioned before, the horizontal velocity depends on the angle of attack α because of the varying air resistance and is thus not constant during the measurements shown in Figure 4. Therefore, lift and drag coefficients c_L and c_D are usually used in aerotechnics, rescaling the forces with the stagnation pressure $\frac{1}{2}\varrho v^2$ resulting from the Bernoulli equation, i.e.

$$c_L = \frac{F_L}{\frac{1}{2}\varrho v^2 c} \qquad \text{and} \qquad c_D = \frac{F_D}{\frac{1}{2}\varrho v^2 c},$$

where c is the chord length of the wing, and v is the air speed. These coefficients are then plotted in a so-called polar diagram as shown in Figure 5. Again, the curve of profile 3 is perfectly symmetric!

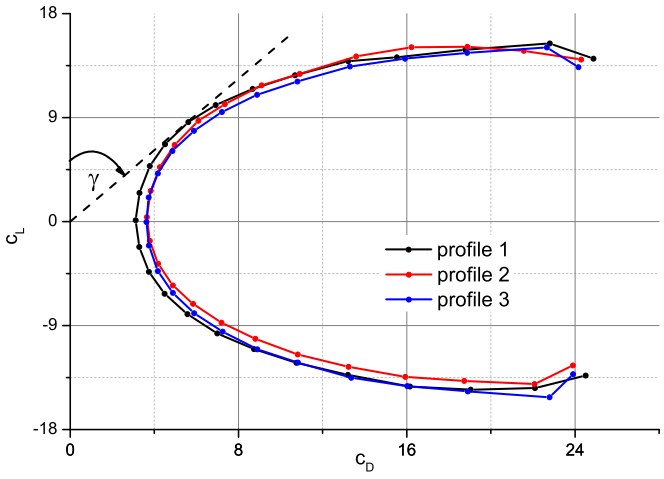

Figure 5: Polar diagrams. The dashed line indicates the best gliding angle γ for profile 1.

In particular, one can immediately read off the best gliding angle γ from these diagrams, that is, the smallest possible angle between the horizontal direction and the wing's trajectory, such that the wing reaches the largest distance for a given loss of height: one has to construct the upper tangents on these curves running through the origin. In the tangent point,

$$\frac{c_D}{c_L} = \frac{F_D}{F_L} = \tan\gamma$$

is obviously minimal. In this regard, profile 1 is superior to the other two profiles as it allows the steepest tangent, compare Figure 5. Many other findings can be derived from the curves in Figure 5, but a detailed discussion would go beyond the scope of this report.

5 Streamlines and turbulence

Streamline patterns are obtained by forming sections of grid points and averaging the velocities (divided by the number of particles) in each section, as shown in Figures 6 and 7.

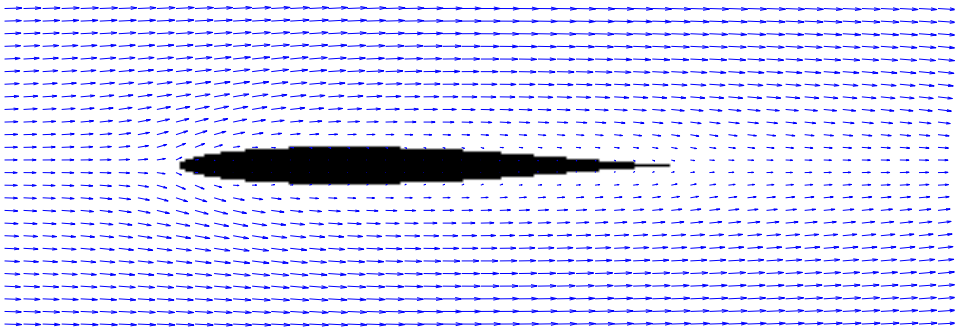

Figure 6: Streamlines for profile 3, at $\alpha = 0°$

Smaller arrows mean that the velocities in this segment add partially up to zero, and thus indicate turbulence phenomena. There is only little turbulence for the symmetric profile 3 in neutral position, but substantial turbulence behind profile 2 and above its rear end for $\alpha = 20°$. However, the method used here is too coarse to investigate the interesting phenomenon of flow separation in greater detail, since one cannot resolve the boundary layer between the wing and the flow properly.

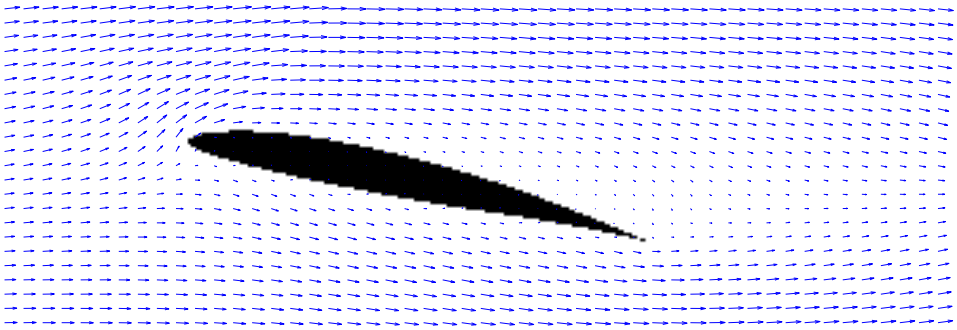

Figure 7: Streamlines for profile 2, at $\alpha = 20°$

6 Conclusions

A wind tunnel simulation using LGCA describes the basic phenomena of lift and drag correctly. Different properties of the airfoils under investigation, such as thickness or symmetry, lead to different results that appear to be coherent, at least in a qualitative way. For a more precise treatment of turbulence phenomena, a considerably higher resolution at the boundary layer is needed. This could be achieved by means of a grid with variable spacing in order to keep the computational effort reasonable, but in turn, the implementation would become much more involved. Eventually, for a wing with finite span, 3dimensional effects would have to be taken into account.

References

[1] U. Frisch, B. Hasslacher, Y. Pomeau: *Lattice-Gas Automata for the Navier-Stokes Equation.* Physical Review Letters. 56, 1986, S. 1505–1508

[2] E. Götsch. *Luftfahrzeugtechnik*, Motorbuchverlag, Stuttgart 2003

[3] H. Schlichting, E. Truckenbrodt. *Aerodynamik des Flugzeuges, Bd. 1*, Springer, Berlin 2001